Comparison of three scattering models for ultrasound blood characterization

Emilie Franceschini, Ratan K Saha, Guy Cloutier

Comparison of three scattering models for ultrasound blood characterization

Emilie Franceschini, *Member IEEE,* Ratan K. Saha, and Guy Cloutier, *Senior Member IEEE,*

Abstract

Ultrasonic backscattered signals from blood contain frequency-dependent information that can be used to obtain quantitative parameters reflecting the aggregation level of red blood cells (RBCs). The approach consists in estimating structural aggregate parameters by fitting the spectrum of the backscattered radio-frequency echoes from blood to an estimated spectrum considering a theoretical scattering model. In this study, three scattering models were examined: a new implementation of the Gaussian Model (GM), the Structure Factor Size Estimator (SFSE) and the new Effective Medium Theory combined with the Structure Factor Model (EMTSFM). The accuracy of the three scattering models in determining mean aggregate size and compactness was compared by two- and three-dimensional (2D and 3D) computer simulations where RBC structural parameters are controlled. Two clustering conditions were studied: (1) when the aggregate size varied and the aggregate compactness was fixed in both 2D and 3D cases, and (2) when the aggregate size was fixed and the aggregate compactness varied in the 2D case. For both clustering conditions, the EMTSFM was found more suitable than the GM and SFSE for characterizing RBC aggregation.

E. Franceschini is with the Laboratoire de Mécanique et d'Acoustique LMA - CNRS UPR 7051, Aix-Marseille University, Centrale Marseille, F-13402 Marseille Cedex 20, France (e-mail: franceschini@lma.cnrs-mrs.fr).

R. K. Saha is with the Saha Institute of Nuclear Physics, Applied Material Science Division, 1/AF Bidhannagar, Kolkata-700 064, India.

G. Cloutier is with the Laboratory of Biorheology and Medical Ultrasonics, University of Montreal Hospital Research Centre (CRCHUM), 2099 Alexandre de Sève (Room Y-1619), Montreal, Quebec H2L 2W5, Canada and with the Department of Radiology, Radio-Oncology and Nuclear Medicine, and Institute of Biomedical Engineering, University of Montreal, Montreal, Quebec, Canada.

Comparison of three scattering models for ultrasound blood characterization

I. Introduction

Quantitative ultrasound (US) techniques are mainly based on the frequency analysis of backscattered signals by biological tissues to determine physical properties of the average tissue microstructure. These techniques rely on theoretical scattering models to fit the spectrum of backscattered echoes to an estimated spectrum using an appropriate model. The theoretical scattering model most frequently used for this purpose is the Gaussian model (GM) [1] [2] that yields two tissue properties: the average scatterer size and the acoustic concentration (i.e., the product of the scatterer number density by the square of the relative impedance difference between scatterers and the surrounding medium). This approach was used to characterize dilute scattering media such as the eye [3], prostate [4] and breast [5]. Blood has also been studied with this technique [6], although estimations could be biased.

An important contribution of ultrasonic blood characterization is to assess the level of red blood cell (RBC) aggregation, which is a surrogate marker of inflammation [7]. It is well known that when RBCs are under low shear rates ($<$10 s^{-1}), they interact strongly with each other and form complex rouleaux or three-dimensional (3D) structures. When the shear rate increases, these rouleaux or compact structures disaggregate. The aggregation phenomenon in human blood is normal, however hyperaggregation is a pathological state associated with several circulatory diseases, such as deep venous thrombosis, atherosclerosis and diabetes mellitus. Blood characterization using US backscatter techniques provides the unique opportunity of monitoring RBC aggregation non-invasively and *in vivo* within blood vessels. This quantification may help to elucidate the role of RBC aggregation in the etiology of such diseases.

US backscatter by blood is mainly due to RBCs that constitute the vast majority (97%) of the blood cellular content. Blood can thus be described as a biphasic fluid composed of RBCs immersed in plasma. Since RBCs are acoustically considered as weak scatterers (impedance contrast between RBCs and plasma being around 13%), multiple scattering can be neglected. However, for such tissue, it is not straightforward to develop a theoretical scattering model because of the high density of RBCs (their volume fraction or hematocrit varies between 30 and 50%) and their ability to form aggregates. The Structure Factor Model (SFM) [8] [9] is an US scattering model proposed to simulate the backscatter coefficient (BSC) of aggregated RBCs. The SFM sums the acoustic contributions from individual RBCs and models their interaction by a statistical mechanics structure factor, which is by definition the Fourier transform of the spatial distribution of RBCs [8] [9]. However, the SFM can hardly be implemented to estimate the structural aggregate parameters in the framework of an inverse problem formulation because of the intensive computational time to assess the structure factor by realizing distributions of aggregating RBCs. That is why Yu and Cloutier [10] developed the SFSE scattering theory that approximates the SFM by

using a second-order Taylor expansion of the structure factor. The SFSE is thus not as accurate as the SFM. The SFSE estimates two physical parameters describing the microstructure of RBC aggregates: the packing factor that increases with erythrocyte clustering and the average aggregate isotropic radius. However, experiments with pig blood in controlled flow devices [10] and 3D numerical simulations of isotropic monodisperse aggregates [11] recently showed that the two indices are correlated and follow a quadratic relationship, thus reducing the BSC parameterization to one structural index.

Another scattering model called the Effective Medium Theory combined with the SFM (EMTSFM) was recently proposed to better approximate the SFM [12]. It assumes that aggregates of RBCs can be treated as individual homogeneous scatterers, which have effective properties determined by the acoustical characteristics and concentration of RBCs within aggregates. The EMTSFM allows characterizing the radius, and for the first time in the quantitative US field, the compactness of RBC aggregates [12]. In the field of clinical hemorheology [13], assessing the compactness of RBC aggregates is of high clinical importance since it is related to the binding energy between cells. Normal RBC aggregates form rouleaux type structures, whereas pathologies associated with stronger binding energies result in clumps of RBCs (close to a spherical isotropic packing) [14] [15].

In our previous study [12], the EMTSFM and the SFM were compared in the framework of a forward problem study to determine the BSC from a known distribution of RBCs with known acoustical parameters. The goodness of the approximation of the EMTSFM in comparison with the SFM was examined as a function of frequency and structural aggregate parameters (aggregate size and compactness). Based on a two-dimensional (2D) simulation study, the EMTSFM was found to approximate the SFM with relative errors less than 30% for a product of the wavenumber times the mean aggregate radius $kr_{ag}\leq$1.32 [12]. The aims of the present paper are :

1) to evaluate the EMTSFM in an inverse problem framework, i.e. to determine RBC structural features from the measured BSC, and
2) to compare the EMTSFM with two other scattering models: the SFSE and a new implementation of the GM slightly modified to treat aggregating scatterers.

To our knowledge, there is no means to experimentally assess aggregate sizes at a normal physiological hematocrit of 40% because RBCs at that hematocrit are opaque to light. It would thus not be feasible to quantitatively evaluate the performance of the different models with real experimental data. In the field of blood imaging and characterization, the assessment of accuracy of a scattering model was only performed at a low hematocrit of 6% by comparing optical and acoustic measurements of RBC aggregate sizes [10]. In the current paper, we thus aim to determine the performance of three theoretical scattering models (the new implementation of the GM, the SFSE and the EMTSFM) to extract the aggregation parameters from computer simulations where RBC structural parameters (such as the hematocrit, the aggregate size and compactness) are known.

The important contribution of the EMTSFM is the parameterization of the BSC with the aggregate compactness [12], which is a structural parameter not available in any other modeling strategies proposed in quantitative US. The potential of the EMTSFM and of the two other scattering models in estimating the aggregate compactness was examined by 2D computer simulations based on the SFM in controlled clustering configurations (when the

aggregate compactness varies and the aggregate radius is fixed). This clustering condition was only conducted in 2D because of the computational load required to generate three-dimensional RBC distributions with various aggregate compactnesses with the SFM [12]. Some 3D computer simulations were also used in the controlled clustering configurations as those performed in 2D (when the aggregate size vary and the aggregate compactness is fixed) in order to compare the BSC behavior between 2D and 3D simulations, and estimated structural aggregate parameters with the three scattering models.

II. Computer simulations based on the Structure Factor Model (SFM)

This section presents computer simulations performed to predict the frequency dependence of the BSC from aggregated RBCs based on the SFM. In the following, it is assumed that the incident wavelength λ is large compared to the RBC size. Consequently, the RBC shape could be approximated by a simple geometry having an equivalent surface in 2D or having an equivalent volume of a RBC in 3D [16]. RBCs were modeled as parallel infinite cylinders in the 2D case and as spheres in the 3D case of radius a, that have small contrast in acoustical properties relatively to the plasma (see Table I). This RBC shape approximation has some limitations for larger frequencies (>20 MHz) and will be discussed later in Section V-C.

The SFM describing US backscatter by biological tissues consists of summing contributions from cells and modeling the cellular interaction by a statistical mechanics structure factor [8] [9]. By considering a collection of N identical and weak scattering RBCs, the BSC expression can be written as:

$$BSC_{SFM}(-2k) = m\sigma_b(-2k)S(-2k), \tag{1}$$

where k is the wavenumber and m the number density of RBCs that is related to the systemic hematocrit ϕ as $m = \phi/A_p$ (where A_p is the RBC area) for 2D modeling, or as $m = \phi/V_p$ (where V_p is the RBC volume) for 3D modeling. The backscattering cross section σ_b of a single weak RBC was calculated using the fluid infinite cylinder expression in the 2D case [12] or using the fluid-filled sphere expression in the 3D case [17] [18] given by:

$$\begin{aligned} \sigma_b(-2k) &= \frac{k^3 A_p^2 \gamma_z^2}{2\pi}\left(\frac{J_1(2ka)}{ka}\right)^2 \quad \text{in the 2D case} \\ &= \frac{k^4 V_p^2 \gamma_z^2}{4\pi^2}\left(3\frac{\sin(2ka) - 2ka\cos(2ka)}{(2ka)^3}\right)^2 \quad \text{in the 3D case} \end{aligned} \tag{2}$$

where J_1 is the first order Bessel function of the first kind and γ_z is the relative impedance difference between the RBC and its suspending medium (i.e., the plasma). The function S is the structure factor representing the spatial positioning of RBCs and is defined by:

$$S(-2k) = E\left[\frac{1}{N}\left|\sum_{i=1}^{N} e^{-i2\mathbf{k}\mathbf{r}_i}\right|^2\right] \tag{3}$$

where E represents the expected value of a random variable and $\mathbf{r}_i$ the position vectors defining the center of the ith RBC in space. In general, the structure factor of a medium containing RBCs distributed in the 2D space (or in the 3D space) can be determined from the 2D Fourier transform (or 3D Fourier transform) of the spatial distribution

of particles (see the Appendix of Ref. [19]).

The computation of the BSC_{SFM} using the SFM requires an intensive computation because of the calculation of the structure factor S as described in Eq. (1). Since the structure factor is by definition a statistical quantity, an average of structure factors from several RBC spatial distributions can give an estimated value of S. Because of the computational load to generate aggregating RBC distributions, a simple and fast method was used to randomly generate non-overlapping RBC aggregates which were isotropic and similar in size. For the 2D and the 3D computer simulations, the simulated BSC_{SFM} were obtained from the method described in section III of Refs. [12] and [11], respectively. Note that 2D simulations are computationally less expensive but significant insights can be gained by studying 2D systems. On the other hand, 3D simulations are intuitively appealing because they better mimic experimental situations but are computationally expensive. These methods are briefly summarized in the following.

Random distributions for aggregating RBCs were computed within the simulated surface area of 600 $\times$ 600 μm^2 in the 2D case and within the simulated volume of 1000 $\times$ 125 $\times$ 125 μm^3 in the 3D case. The RBC radius a was set to 2.75 μm for all simulations. We first specified the systemic hematocrit ϕ, the aggregate radius r_{ag} and the aggregate compactness ϕ_i (i.e. the RBC concentration within aggregate). Aggregates of identical radii r_{ag} and of identical compactness ϕ_i were then randomly distributed with non-overlapping positions to give the desired concentration of aggregates $\phi_{ag} = \phi/\phi_i$. Note that in the case of the 3D study, a small number of non-aggregated RBCs was added to reach the desired systemic hematocrit. It means that all the RBCs were aggregated in blood in the 2D case, whereas a fraction of RBCs were aggregated while the rest remained disaggregated in the 3D case. Finally, RBC distributions within aggregates were then generated as follows:

- in the 2D case, the locations of the RBCs were generated using external and repulsive forces to obtain random RBC positions inside each aggregate, such that the distribution of RBCs within each aggregate was different [12]. This technique allowed to study several aggregation configurations (1) when the aggregate size varied and the aggregate compactness was fixed to 0.6, and (2) when the aggregate compactness varied from 0.3 to 0.6 and the aggregate size was fixed.
- in the 3D case, the RBCs were stacked by following a hexagonal close packing (HCP) structure for each aggregate, such that the distribution of RBCs within each aggregate was identical. This HCP structure provides the highest compactness that is about 0.74 for spheres [11]. Therefore, this technique allowed to study several aggregation configurations when the aggregate size varied and the aggregate compactness was fixed to 0.74.

For each distribution of RBCs, the 2D or 3D Fourier transformation of the spatial organization of RBCs was then computed to obtain the corresponding structure factor. A mean structure factor was determined from 400 different tissue realizations in the 2D case (see section III.B in Ref. [12]) and from 250 different tissue realizations in the 3D case (see section III.B in Ref. [11]).

III. Ultrasound backscattering modeling for the estimation of structural aggregate parameters

As seen previously in section II, the SFM allows to simulate the BSC from RBCs whatever the RBC spatial distribution (i.e. disaggregated or aggregated RBCs and/or with various aggregate sizes and compactnesses). However, the SFM can hardly be implemented to estimate structural parameters in the framework of an inverse problem formulation because of the intensive computational time to assess the structure factor by realizing distributions of RBCs with simulations. That is why two scattering theories, named the SFSE and the EMTSFM, have been recently developed to approximate the SFM for practical assessments of RBC structural features (i.e., in an inverse problem formulation). This section presents these two scattering theories (the SFSE and the EMTSFM) as well as the GM also used for tissue characterization. In this work, we present a new implementation of the GM model inspired by our development on EMTSFM. All three theories fit a curve to the simulated BSC_{SFM} from blood to estimate aggregation parameters using the minimization routine *"fminsearch"* in MATLAB (The MathWorks, Inc., Natick, MA), i.e. a Nelder-Mead simplex method. Note that this fit was realized in the frequency bandwidth from 4 MHz to the frequency corresponding to the first minimum of the BSC_{SFM} (i.e., after the frequency-dependent increase in BSC followed by a peak and a reduction to its first minimum).

A. The Structure Factor Size Estimator (SFSE)

The SFSE developed by Yu and Cloutier [10] approximates the SFM with a second-order Taylor expansion of the structure factor in k as follows:

$$\begin{aligned} S(-2k) &\approx W - 4(kR_g a)^2 \qquad \text{in the 2D case} \\ &\approx W - 4(kR_g a)^2 \approx W - \frac{12}{5}(kR_{sp}a)^2 \qquad \text{in the 3D case} \end{aligned} \tag{4}$$

where W is the low-frequency limit of the structure factor ($S(k)|_{k\to 0}$) called the packing factor [20] [21] and R_g is the radius of gyration of RBC aggregates assumed to be isotropic and expressed in number of RBCs [10]. Note that in the 3D case, R_g is related to the isotropic radius R_{sp} of an aggregate (expressed in number of RBCs) by $R_g = \sqrt{\frac{3}{5}}R_{sp}$ [11] [22]. By assuming identical RBCs, and recombining Eqs. (1) and (4), the SFSE model approximates the BSC as follows:

$$\begin{aligned} BSC_{SFSE}(-2k) &= \frac{1}{2\pi}mk^3A_p^2\gamma_z^2\left(\frac{J_1(2ka)}{ka}\right)^2\left(W - 4(kR_g a)^2\right) \qquad \text{in the 2D case} \\ &= \frac{1}{4\pi^2}mk^4V_p^2\gamma_z^2\left(3\frac{\sin(2ka) - 2ka\cos(2ka)}{(2ka)^3}\right)^2\left(W - \frac{12}{5}(kR_{sp}a)^2\right) \qquad \text{in the 3D case} \end{aligned} \tag{5}$$

The SFSE assumes that the hematocrit ϕ, the RBC radius a and the acoustical properties of plasma and RBCs are known *a priori*. Therefore, Eq. (5) presents only two unknowns that characterize the aggregate structure: W and R_g (or equivalently, W and R_{sp} in the 3D case). Estimated values of W^* and R_g^* (or equivalently, W^* and R_{sp}^* in the 3D case) were determined by fitting the simulated BSC_{SFM} given by Eq. (1) with BSC_{SFSE} given by Eq. (5).

B. The Effective Medium Theory Combined with the Structure Factor Model (EMTSFM)

The EMTSFM assumes that all the scatterers are aggregated, that the aggregates are identical and isotropic and that the scatterers within aggregates are evenly distributed [12]. In the case of blood backscatter, the model consists of treating the RBC aggregates as individual homogeneous particles of radius r_{ag}. These homogeneous particles are characterized by a density ρ_{ag} and a compressibility κ_{ag} derived from the acoustical properties of the two fluids constituting them (i.e., ρ_1, ρ_2, κ_1 and κ_2, where 1 indicates properties of RBCs and 2 those of plasma), and from the internal concentration of RBCs within the aggregates, defined as the aggregate compactness ϕ_i, as follows:

$$\begin{aligned} \rho_{ag} &= \phi_i\rho_1 + (1-\phi_i)\rho_2 \\ \frac{1}{\kappa_{ag}} &= \frac{\phi_i}{\kappa_1} + \frac{1-\phi_i}{\kappa_2} \end{aligned} \tag{6}$$

The BSC from blood is then obtained by summing contributions from individual effective particles of radius r_{ag} and modeling the effective particle interaction by a statistical mechanics structure factor S_{ag}. The equivalent BSC expression is thus given by [12]:

$$BSC_{EMTSFM}(-2k) = m_{ag}\sigma_{ag}(-2k)S_{ag}(-2k), \tag{7}$$

where S_{ag} is the structure factor of a collection of N_{ag} identical particles of radius r_{ag} randomly distributed and m_{ag} is the number density of aggregates that is related to the effective aggregate concentration ϕ_{ag}. The effective aggregate concentration is equal to the RBC concentration in blood ϕ divided by the aggregate compactness ϕ_i: $\phi_{ag} = \phi/\phi_i$. The backscatter cross-section of an effective single particle σ_{ag} was calculated using the fluid infinite cylinder expression in the 2D case [12] or using the fluid-filled sphere expression in the 3D case [17] [18] given by:

$$\begin{aligned} \sigma_{ag}(-2k) &= \frac{k^3\pi r_{ag}^4\gamma_{z_{ag}}^2}{2}\left(\frac{J_1(2kr_{ag})}{kr_{ag}}\right)^2 \quad \text{in the 2D case} \\ &= \frac{4k^4 r_{ag}^6\gamma_{z_{ag}}^2}{9}\left(3\frac{\sin(2kr_{ag}) - 2kr_{ag}\cos(2kr_{ag})}{(2kr_{ag})^3}\right)^2 \quad \text{in the 3D case} \end{aligned} \tag{8}$$

where z_{ag} is the impedance of the equivalent particle and $\gamma_{z_{ag}}$ the relative impedance difference between the equivalent particle and the plasma ($\gamma_{z_{ag}} = (z_{ag} - z_2)/z_2$). For a random distribution of hard-cylinders in 2D, the structure factor was numerically computed as described in the appendix A. For a random distribution of hard-spheres in 3D, the structure factor can be analytically calculated as established by Wertheim [23]. The analytical expression for the structure factor in the 3D case is described in the appendix B.

By assuming that the hematocrit ϕ, the RBC radius a and the acoustical properties of plasma and RBCs are known *a priori*, the unknown parameters are the radius of aggregates r_{ag} and their compactness ϕ_i. The unknown parameters were estimated by matching the simulated BSC_{SFM} given by Eq. (1) with the theoretical BSC_{EMTSFM} given by Eq. (7).

C. The Gaussian Model (GM)

Using the GM, the BSC is modeled with a spatial autocorrelation function describing the shape and distribution of scatterers in the medium. The scattering sites are assumed to be randomly distributed and of simple geometric

shapes, represented as gaussian scatterers mimicking continuous changes in impedance. In this framework, the BSC can be written as the product of the theoretical BSC under Rayleigh scattering and the backscatter form factor (see Eqs. (74)-(76) of Ref. [18] for the GM formulation in 3D). The form factor describes the frequency dependence of BSC attributed to the size and shape of the prototype scatterer. The Gaussian form factor has been used for many applications [3]–[6]. It represents tissue structures as continuously varying distributions of acoustic impedance fluctuations about the mean value, and the effective radius is related to the impedance distribution of the scatterers.

The BSC for the GM formulation is written as the product of the BSC in the Rayleigh limit and the backscatter form factor as follows [18]:

$$\begin{aligned} BSC_{GM}(-2k) &= \frac{k^3 S_s^2 n_z}{2\pi} e^{-2k^2 d^2} = \frac{\pi k^3 a_{eff}^4 n_z}{2} e^{-k^2 a_{eff}^2} \qquad \text{in the 2D case} \\ &= \frac{k^4 V_s^2 n_z}{4\pi^2} e^{-2k^2 d^2} = \frac{4k^4 a_{eff}^6 n_z}{9} e^{-0.827 k^2 a_{eff}^2} \qquad \text{in the 3D case} \end{aligned} \tag{9}$$

where n_z is the acoustic concentration (i.e., the product of the number density of scatterers times the square of the relative impedance difference γ_z between scatterers and the surrounding tissue). In the 2D case (or respectively in the 3D case), the characteristic dimension d is related to the area of the effective scatterer S_s by: $S_s = 2\pi d^2$ (or related to the volume of the effective scatterer V_s by: $V_s = (2\pi d^2)^{3/2}$). Continuous isotropic media can be characterized by the correlation distance d, in the same way as discrete isotropic media are characterized by a scatterer radius [18]. The effective radius of the scatterer a_{eff} is related to the correlation distance d by setting values of S_s (or V_s, respectively) for a continuum model equal to the area of an effective cylinder (or equal to the volume of an effective scatterer) of radius a_{eff}: $S_s = 2\pi d^2 = \pi a_{eff}^2$ or $V_s = (2\pi d^2)^{3/2} = (4/3)\pi a_{eff}^3$.

Estimates of the effective radius a_{eff}^* and acoustic concentration n_z^* were determined by fitting the simulated BSC_{SFM} given by Eq. (1) with BSC_{GM} given by Eq. (9). Effective radii a_{eff} estimated with the GM have been hypothesized to be related to the aggregate radii, and the acoustic concentration n_z is postulated to be the product of the number density of aggregates times the square of the relative impedance difference between aggregates and the plasma as follows:

$$\begin{aligned} n_z &= \gamma_{z_{ag}}^2 \frac{\phi_{ag}}{\pi a_{eff}^2} = \left(\frac{z_{ag} - z_2}{z_2}\right)^2 \frac{\phi}{\phi_i \pi a_{eff}^2}, \qquad \text{in the 2D case} \\ &= \gamma_{z_{ag}}^2 \frac{3\phi_{ag}}{4\pi a_{eff}^3} = \left(\frac{z_{ag} - z_2}{z_2}\right)^2 \frac{3\phi}{4\phi_i \pi a_{eff}^3}, \qquad \text{in the 3D case} \end{aligned} \tag{10}$$

where z_{ag} is the effective impedance of the aggregates approximated by the mixing law: $z_{ag} = \phi_i z_1 + (1 - \phi_i) z_2$. Since the hematocrit ϕ and the acoustical properties of plasma and RBCs are assumed to be known *a priori*, the aggregate compactness can be deduced from the estimated parameters a_{eff}^* and n_z^* by using Eq. (10) as follows:

$$\begin{aligned} \phi_i^* &= \frac{\pi {a_{eff}^*}^2 n_z^* z_2^2}{\phi (z_2 - z_1)^2} \qquad \text{in the 2D case} \\ &= \frac{4\pi {a_{eff}^*}^3 n_z^* z_2^2}{3\phi (z_2 - z_1)^2} \qquad \text{in the 3D case} \end{aligned} \tag{11}$$

It means that the new proposition of the GM was employed in our study as an effective medium model, but contrary to the EMTSFM, the GM is not combined with the SFM (such that the GM is assumed to be accurate only at low

systemic hematocrits). In the following, we thus give the estimated parameters a^*_{eff} and ϕ^*_i with the GM, instead of the classical estimated parameters a^*_{eff} and n^*_z.

IV. Results

This section gives the results of the inverse problem obtained for 2D and 3D computer simulations with the three backscattering models aforementioned: SFSE, EMTSFM and GM.

A. Results obtained from the 2D computer simulations

For the 2D computer simulations, we first studied clustering configurations where the aggregate compactness was fixed to ϕ_i=60% and the aggregate radius r_{ag}/a varied, and then clustering configurations where the aggregate radius was fixed to r_{ag}/a=6.32 and the aggregate compactness ϕ_i varied.

1) Results for the SFSE: The SFSE was first examined for systemic hematocrits of 10, 20 and 30% when the aggregate size varied and the aggregate compactness was fixed to a high value: ϕ_i=60%. Figure 1 shows BSC_{SFM} as a function of frequency for different aggregate sizes and systemic hematocrits. The symbols represent the BSC_{SFM} computation for the disaggregated case (r_{ag}/a=1) and for aggregation with radii r_{ag}/a=3.16, 5.0 and 7.07. Also represented in dashed lines in Fig. 1 are corresponding BSC_{SFSE} fitted curves. The first peaks of the simulated BSC_{SFM} occur at lower frequencies as the aggregate radius increases. Since the fitting curves with the SFSE were realized in the frequency bandwidth from 4 MHz to the frequency corresponding to the first minimum of the BSC_{SFM} (except for the disaggregated case for which the frequency bandwidth is from 4 to 50 MHz), the bandwidth used for the fitting becomes smaller as the aggregate radius increases. It is clear from the figure that the SFSE provided better fits for the lower hematocrit of 10%. As the hematocrit increases, the SFSE model is insufficient to predict the behavior of BSC_{SFM}, especially in the low frequency range. The estimated values of W^* and R^*_g are given in Table II for systemic hematocrits of 10, 20 and 30%. In this table, the relative error for parameter R^*_g corresponds to: $\epsilon_{R^*_g} = \left(R^*_g - (r_{ag}/a)\right)/(r_{ag}/a)$. Figure 2a shows the estimated values of R^*_g as a function of the actual aggregate radii r_{ag}/a for all hematocrits. Also represented are the corresponding linear regression lines showing good correlation $r^2 \geq 0.95$ at all hematocrits. For radii r_{ag}/a between 4.47 and 7.95, relative errors $\epsilon_{R^*_g}$ were less than 30% for hematocrits of 10 and 20%. It is interesting to notice that estimated parameters W^* and R^*_g follow a linear relation for all hematocrits (see Fig. 2b).

The SFSE was also evaluated at systemic hematocrits of 10 and 20% when the aggregate size r_{ag}/a was fixed to 6.32 and the aggregate compactness ϕ_i varied from 30 to 60%. It is important to emphasize that 2D random particle distributions could be easily generated using a random number generator up to an area fraction of approximatively 0.5. For the 20% systemic hematocrit, aggregate compactnesses smaller than 40% could not be computed because the corresponding area fractions of aggregates were too high: $\phi_{ag} > 0.5$. Similarly, the variation of the aggregate compactness could not be performed at a systemic hematocrit of 30% because the area fractions of aggregates is already equal to 0.5 for an aggregate compactness ϕ_i=60%. Figure 3 displays BSC_{SFSE} in dashed lines for the following clustering conditions: r_{ag}/a=6.32 and ϕ_i varying from 30 to 60%. One can notice large differences

between simulated and fitted SFSE curves, especially at low frequencies where the fitted curves over-estimate the BSC_{SFM} amplitude. These differences are larger at ϕ=20%. The estimated values of R_g^* for different aggregate compactnesses are plotted in Fig. 4a. Although the true radius is fixed, estimated R_g^* increases with the aggregate compactness at both hematocrits. We found no correlation between the actual fixed radius and the estimated radii (r^2 <0.06). Notice the linear relation between W^* and R_g^* when the aggregate compactness varies (see Fig. 4b), as observed previously in Fig. 2b when the aggregate radius r_{ag}/a was changed.

2) Results for the EMTSFM: The BSC curves fitted with the EMTSFM are shown in solid lines in Fig. 1 for the case of varying values of r_{ag}/a, and in Fig. 3 for varying ϕ_i. In both cases, the EMTSFM provided good fittings to the simulated BSC_{SFM} curves for all systemic hematocrits. For the clustering conditions where the aggregate radius varied and the aggregate compactness was constant, the estimated values r_{ag}^*/a and ϕ_i^*, and corresponding relative errors are given in Fig. 5 for systemic hematocrits of 10, 20 and 30%. For the clustering conditions where the aggregate compactness varied and the aggregate radius was constant, the results are shown in Fig. 6 for systemic hematocrits of 10 and 20%. For the EMTSFM, the relative errors for each parameter correspond to:

$$\epsilon_{r_{ag}^*} = \frac{(r_{ag}^*/a) - (r_{ag}/a)}{(r_{ag}/a)} \quad \text{and} \quad \epsilon_{\phi_i^*} = \frac{\phi_i^* - \phi_i}{\phi_i}. \tag{12}$$

In both sub-studies where the aggregate radius and compactness varied, a very good correspondence can be observed between true and estimated aggregate sizes and compactnesses. The relative errors for the estimated aggregate radii and compactnesses were less than 13% and 14%, respectively, for all hematocrits and for all studied aggregating configurations.

3) Results for the GM: Figure 7 presents the BSC_{SFM} curves fitted with the GM for several aggregate sizes at the same clustering conditions as in Fig. 1. The GM provided over-estimates in the low frequency range for all systemic hematocrits. Excellent correlations (r^2 ≥0.92) were found between the estimated and true aggregate radii for all hematocrits (data not shown). The estimated values a_{eff}^*/a and ϕ_i^* from the GM, and corresponding relative errors are given in Fig. 8. For systemic hematocrits of 10 and 20%, the estimated radii and compactnesses are quantitatively satisfactory with relative errors less than 15%. However, for ϕ=30%, the relative errors increase up to 40%.

For the clustering conditions where the aggregate compactness varied and the aggregate radius was constant, the results are shown in Fig. 9 for systemic hematocrits of 10 and 20%. As previously observed with the SFSE, the estimated effective radius increases as the aggregate compactness increases. The estimated radii and compactnesses matched the true parameters at ϕ=10% with relative errors less than 17%. However, for ϕ=20%, large relative errors (up to 74%) were obtained.

4) Comparison of the errors between the simulated BSC and the fitted curves with the three scattering models: The errors (i.e. differences) between the simulated BSC and the fitted curves with the three scattering models (SFSE, EMTSFM and GM) are presented in Fig. 10. The logarithm of the error is shown to enhance reading. The error reveals how the models fit the data. It is clear from the figure that errors were smaller with the EMTSFM and larger with the GM, for each hematocrit. For the aggregating conditions where the aggregate radius varied, the

error decreases as the radius increases. When the aggregate radius increases, the bandwidth frequency used for the fit becomes smaller and therefore, the number of frequencies used for the error computation decreases.

B. Results obtained from the 3D computer simulations

For the 3D computer simulations, the GM, SFSE and EMSTFM were examined when the aggregate size varied and the aggregate compactness was fixed to a high value: ϕ_i=74%.

It is important to note that the 3D simulated aggregates were highly packed leaving small numbers of particles as non-aggregated RBCs. For each tissue realization, the actual mean aggregate radius r_{ag} was computed using Eq. (6) in Ref. [11], and then the concentration of aggregated RBCs ϕ' was computed as:

$$\phi' = \frac{\phi_i N_{ag}(4/3)\pi r_{ag}^3}{1000 \times 125 \times 125 \times (10^{-6})^3}. \tag{13}$$

Figure 11a shows the values of ϕ' as a function of the mean aggregate radius r_{ag}/a for the three systemic hematocrits of 20, 30 and 40%. The percentage of disaggregated RBCs was between 20 and 30% for the systemic hematocrit of 20% and between 27 and 37% for the systemic hematocrit of 40%. Note that the three models presented in section III assumed that all RBCs were aggregated in blood and that aggregates had identical shape and size. Consequently, during the inversion procedure of the 3D BSC data, we neglected the contribution of the disaggregated RBCs on the simulated BSC_{SFM} and we replaced the hematocrit ϕ by the value of the concentration of aggregated RBCs ϕ'.

Figure 11b and c shows BSC_{SFM} as a function of frequency for several aggregate sizes and systemic hematocrits of 30 and 40%. Also represented in Fig. 11b and c are corresponding fitted curves obtained with the SFSE, EMTSFM and GM. The fitted GM and SFSE curves did not produce good fits to the 3D data and overestimated the BSC_{SFM} amplitude (especially in the low frequency range), as observed in the 2D case (see Figures 1 and 7). At the opposite, the EMTSFM provided good fittings to the simulated BSC_{SFM} curves.

The results obtained with the SFSE were already presented in a previous article [11]. Excellent correlations ($r^2 \geq$0.94) were found between the estimated and true aggregate radii for all hematocrits (see Fig. 5a in Ref. [11]). It can also be seen in Fig. 5a of Ref. [11] that for each hematocrit there is an aggregate size range where the SFSE method works at its best. For example, relative errors for estimated radii were less than 20% for true radius values between 14 and 17 μm at the hematocrit of 40%. The parameters W^* and R_{sp}^* followed a quadratic relationship (as in Fig. 5b of Ref. [11]).

Figure 12 gives the values of r_{ag}^* and ϕ_i^* estimated with the EMTSFM and corresponding relative errors that were less than 15% and 23%, respectively, for all hematocrits. Figure 13 gives the values of a_{eff}^* and ϕ_i^* estimated with the GM and corresponding relative errors. The estimated radii with the new formulation of the GM are quantitatively satisfactory with relative errors less than 9% for all hematocrits. The relative errors for the estimated compactnesses with the GM are larger with relative errors up to 32% for the hematocrits of 20 and 30%, and up to 76% for the hematocrit of 40%.

V. Discussion and conclusions

Three scattering models for the characterization of RBC aggregation were examined. From these models, the gold standard simulated BSC_{SFM} was fitted and aggregation parameters were extracted. The SFSE has been developed for blood characterization and the GM is a model that has been used in various tissue studies. Herein, the radius estimates R_g from the SFSE and a_{eff} from the GM were hypothesized to represent the aggregate size.

A. Clustering conditions where the aggregate radius varied and the aggregate compactness was constant (2D and 3D computer simulations)

The 2D and 3D computer simulations were performed on the same clustering configuration where the aggregate radius varied and the aggregate compactness was constant. It is interesting to observe the same BSC_{SFM} behavior for both 2D and 3D studies. Indeed, the simulated BSC_{SFM} amplitude increases with the size of aggregates and the BSC_{SFM} first peaks occur at lower frequencies as the aggregate radius increases (see Fig. 1 in the 2D case, and Fig. 11b and c of the present paper and Fig. 4 of Ref. [11] in the 3D case). Moreover, as it can be observed in Figures 1 and 7 in the 2D case and in Figure 11 in the 3D case, the data fitting quality obtained with the three models were quite similar. In both 2D and 3D cases, it is clear that the GM and the SFSE are insufficient to model the complex behavior of BSC and that the EMTSFM was the model that better fitted the BSC data for all studied hematocrits.

Although the SFSE model did not produce good spectral fits to the BSC data for 2D and 3D computer simulations, significant correlations were found between the estimated and true radii with r^2 superior to 0.95 at all hematocrits (see Fig. 2a in the present paper and see Fig. 5a of Ref. [11]). However, the estimated aggregation parameters W^* and R_g^* followed a linear relationship in our 2D simulation study. This relation was also found to be quadratic in 3D numerical simulations [11] and under experimental conditions [10]. It means that the BSC parameterization can be reduced to one parameter and that no new information can be obtained with the parameter W^*.

The EMTSFM and the GM used as effective medium models gave quantitatively satisfactory radius estimates with relative errors less than 15% for the 10 and 20% hematocrits in the 2D case, and for all hematocrits in the 3D case. For the highest systemic hematocrit, the aggregate compactnesses were better estimated with the EMTSFM with relative errors less than 14% in the 2D case (and less than 23% in the 3D case), whereas the relative errors were between 19 and 36% in the 2D case (and between 59 and 76% in the 3D case) for the GM. These results with the EMTSFM and the GM were somewhat anticipated since the assumption of a random distribution of scatterers used by the GM fails due to the spatial correlation between scatterers in a dense medium [24]. To conclude, the EMTSFM was more suitable than the GM and SFSE for characterizing the aggregate microstructure in both 2D and 3D studies.

B. Clustering conditions where the aggregate compactness varied and the aggregate radius was constant (2D computer simulations)

For the highest simulated hematocrit of 20%, the aggregate radii normalized by the RBC radius were estimated between 4.34 and 8.55 using the SFSE model and between 3.83 and 5.33 using the GM (see Fig. 4a and Fig. 9), whereas the actual aggregate radius was r_{ag}/a=6.32. Therefore, we found no correlation between the actual fixed aggregate radius and the estimated radii. The GM and SFSE cannot take into account a variation in the aggregate compactness at a large hematocrit, since it is interpreted as a change in the aggregate size.

In the case of the SFSE, one could have expected a fixed value of the estimated radius R_g^* and a variation of the estimated packing factor W^*, when the aggregate radius was fixed and the aggregate compactness varied. However, both R_g^* and W^* increased as the true aggregate compactness was raised. The estimated parameters R_g^* and W^* followed linear relations for all hematocrits (see Fig. 4b), as observed previously in Fig. 2b when the aggregate radius r_{ag}/a was changed. It means that W^* and R_g^* carry the same information and that the BSC parametrization is reduced to one parameter.

The estimated parameters using the EMTSFM presented in Fig. 6 show that the model gave quantitatively satisfactory estimates for all aggregate compactnesses and for all studied hematocrits. Contrary to the GM and SFSE, the EMTSFM provided a quasi-constant aggregate radii between 5.7 and 5.9 for both studied hematocrits. Moreover, the aggregate compactnesses were estimated with relative errors less than 12% at both studied hematocrits for that model. The errors between simulated BSC_{SFM} and the fitted curves were also smaller with the EMTSFM, as it can be observed in Fig. 10b. To conclude, the EMTSFM was the model that explained better the simulated BSC_{SFM}.

C. Computation of RBC distributions and of BSC_{SFM}

The two methods we used here to obtain the RBC spatial distributions did not take into consideration realistic interactions between RBCs. These methods were already presented in Ref. [12] and [11] for the 2D and 3D computer simulations, respectively. They were simple and fast methods to generate samples containing non-overlapping, identical and isotropic aggregates. The 3D computer simulations allowed to better mimic real data but they are time consuming (see section III.A and section V of Ref. [11] to obtain a quick review of different approaches to simulate compact RBC aggregates). In order to simulate the BSC data with the SFM reference model, the method we chose to distribute RBCs in the 3D case allowed (1) to study various aggregate sizes with the same aggregate compactness and (2) to reach the physiological hematocrit of 40% by mixing identical RBC aggregates and disaggregated RBCs. Since studied scattering models assumed that all RBCs were aggregated in blood and since the averaged percentage of disaggregated RBCs was small (around 25%), the influence of the disaggregated RBCs on the simulated BSC_{SFM} was neglected during the inversion procedure of the 3D BSC data. Contrary to the 3D modeling, the method we chose to distribute RBCs in the 2D case allowed (1) to study the clustering condition where the aggregate compactness vary and the aggregate size is fixed and (2) to have only aggregated RBCs in blood. However, the 2D computer simulations were limited to a maximum hematocrit of 30% because of

the difficulty to simulate with the SFM values greater than 30%. To clarify, the main difficulty in the 2D case was to distribute compact aggregates and to have only aggregated RBCs in blood. The maximum value of the aggregate area fraction $\phi_{ag_{max}}$ was fixed to 0.5, corresponding to the maximum particle area fraction that can be easily generated using a random number generator. The procedure we chose to distribute the RBCs within aggregates allows reaching a maximum value of aggregate compactness $\phi_{i_{max}}$ equal to 0.6 (see section III.B. in Ref. [12]). As a consequence, the maximum value of the systemic hematocrit was limited to: ϕ_{max}= $\phi_{ag_{max}}$ $\phi_{i_{max}}$=0.3.

We also modeled individual biconcave RBCs as spheres of equivalent volume in the 3D study and studied BSC between 4 and 45 MHz. The impact of modeling a RBC by a sphere on the frequency dependence of the backscatter cross-section has been studied and errors are introduced above 20 MHz [16] [25]. The impact of this simplification on the simulated BSC_{SFM} and structural aggregate estimates with the three models (SFSE, GM and EMTSFM) is unknown and still needs to be explored.

D. On the use of the EMTSFM in vivo

The EMTSFM assumes that all RBCs are aggregated in blood and that aggregates are identical and isotropic. Therefore, the BSC behavior obtained in our simulations have pronounced frequency peaks. In experimental conditions [10], the BSC behavior was smoother and the peaks were less pronounced. The reason behind this might be that real blood contains several sizes of aggregates, and since the location of BSC peaks are different for different aggregate populations, a relatively smoother BSC curve can be obtained. Another important aspect to consider is the assumption of isotropic aggregates. In human blood, low shear rates can promote the formation of RBC aggregates having anisotropic (i.e. rouleaux) or isotropic (i.e. clump) structures. The rouleaux like pattern is typically associated to normal blood. However, as the binding energy between RBCs increases with inflammation [26], aggregates form clump structures such as in diabetes mellitus [14] [15]. The assumption of isotropic aggregates in the EMTSFM is thus valid as far as we are concerned with the study of pathological states. In the case of normal human rouleaux of RBCs, if the EMTSFM is applied to estimate structural parameters such as the aggregate size and compactness, this assumption would obviously create a bias against the parameter estimation. Therefore, future improvements should consider incorporating the aggregate anisotropy and the polydispersity in terms of aggregate size and compactness to provide an optimal model for the inversion of experimental data. Future validations will also evaluate the EMTSFM in a controlled Couette flow experiment with ghost RBCs (i.e., optically visible RBCs with no hemoglobin and viable membrane properties) coated with dextran polymers to change attractive energies between erythrocytes and thus modulate the aggregate compactness and size.

Another difficulty to apply the EMTSFM *in vivo* is that the spectral content of backscattered echoes is also affected by attenuation caused by intervening tissue layers (such as the skin) between the probe and the blood flow. To evaluate correctly microstructural parameters, it is thus of major interest to take into account tissue attenuation effects. Note that the SFSE was slightly modified to introduce the attenuation term in the BSC expression and was named the Structure Factor Size and Attenuation Estimator (SFSAE) [27]. The SFSAE allows to determine simultaneously

blood structural parameters (i.e., W^* and R_g^*) and the total attenuation [28] [29]. Future improvements of the EMTSFM should incorporate the tissue attenuation as for the SFSAE. It means that the EMTSFM should be slightly modified by introducing the attenuation term to estimate simultaneously the RBC aggregate size, compactness and the total attenuation.

APPENDIX A
NUMERICAL COMPUTATION OF THE STRUCTURE FACTOR S_{ag} FOR HARD-CYLINDERS IN 2D

Since there is no analytical expression of the structure factor S_{ag} for hard-cylinders in 2D [30] [31], S_{ag} was numerically computed for several values ϕ_{ag} varying from 0.01 to 0.5 with a step of 0.01. It means that, in the 2D case, the cylinder concentration ϕ_{ag} was rounded to the second decimal for the computation of S_{ag} in Eq. (7). Note that the computation of S_{ag} depends not only on the area fraction ϕ_{ag} but also on the effective particle radius r_{ag}. That is why S_{ag} that depends on r_{ag} was computed in a dimensionless way as described next.

For each specified value of ϕ_{ag}, aggregates of an arbitrarily normalized (dimensionless) radius of $1/60$ were randomly distributed within a dimensionless surface area $L'^2 = 1 \times 1$ using a random number generator with non-overlapping positions. The corresponding density matrix D' was computed by dividing the square simulation plane L'^2 in N_p^2 pixels (herein, N_p=512) and by counting the number of particles falling into each pixel. The Fourier transformation of the density matrix D' was then computed to generate a structure factor S_{ag}. A mean S_{ag} was determined by repeating 400 times this procedure. When the value of the effective particle radius r_{ag} was specified, the centered grid of wavevectors for the structure factor S_{ag} was computed between $\pm\dfrac{\pi N_p}{2 \times 60 r_{ag}}$ with a step of $\Delta k = \dfrac{\pi}{60 r_{ag}}$ (i.e., by putting the simulated surface length $L' = 60 r_{ag}$).

APPENDIX B
ANALYTICAL EXPRESSION OF THE STRUCTURE FACTOR S_{ag} FOR HARD-SPHERES IN 3D

The structure factor S for hard-spheres is given by [23] [32]

$$S(k) = \frac{1}{1 - 4\pi m d^3 \int_0^1 z^2 \frac{sin(2kz)}{2kz} c(z) dz} \tag{14}$$

where m is the number density of hard-spheres, d is the hard-sphere diameter and $c(z)$ is the direct correlation function given by [23] [32]:

$$\begin{aligned} -c(z) &= c_0 + c_1 \frac{z}{d} + c_3 \left(\frac{z}{d}\right)^3 \qquad \text{for } z \leq d \\ &= 0 \qquad\qquad\qquad\qquad\qquad\quad \text{for } z > d \end{aligned} \tag{15}$$

The coefficients c_0, c_1 and c_3 are given by [23] [32]

$$\begin{aligned} c_0 &= \frac{(1+2\phi)^2}{(1-\phi)^4} \\ c_1 &= -\frac{6\phi(1+\phi/2)^2}{(1-\phi)^4} \\ c_3 &= \frac{\phi}{2} c_0 = \frac{\phi(1+2\phi)^2}{2(1-\phi)^4} \end{aligned} \tag{16}$$

ACKNOWLEDGMENTS

This work was supported by the Fonds Incitatifs Recherche of the Université de Provence and by an operating grant from the Canadian Institutes of Health Research (♯MOP-84358).

REFERENCES

[1] F. L. Lizzi, M. Ostromogilsky, E. J. Feleppa, M. C. Rorke, and M. M. Yaremko, "Relationship of ultrasonic spectral parameters to features of tissue microstructure", IEEE Trans. Ultrason. Ferroelect. Freq. Contr., vol. 33, pp. 319-329, 1986.

[2] M. F. Insana, R. F. Wagner, D. G. Brown and T. J. Hall, "Describing small-scale structure in random media using pulse-echo ultrasound", J. Acoust. Soc. Am., vol. 87, no. 1, pp. 179-192, 1990.

[3] E. J. Feleppa, F. L. Lizzi, D. J. Coleman, and M. M. Yaremko, "Diagnostic spectrum analysis in ophthalmology: a physical perspective", Ultrasound Med. Biol., vol. 12, pp. 623-631, 1986.

[4] E. J. Feleppa, T. Liu, A. Kalisz, M. C. Shao, N. Fleshner, and V. Reuter, "Ultrasonic spectral-parameter imaging of the prostate", Int. J. Imag. Syst. Technol., vol. 8, pp. 11-25, 1997.

[5] M. L. Oelze, W. D. O'Brien, J. P. Blue, and J. F. Zachary, "Differentiation and characterization of rat mammary fibroadenomas and 4T1 mouse carcinomas using quantitative ultrasound imaging", IEEE Trans. Med. Imaging, vol. 23, pp. 764-771, 2004.

[6] H. Kitamura, B. Sigel, J. Machi, E. J. Feleppa, J. Sokil-Melgar and J. Justin, "Roles of hematocrit and fibrinogen in red cell aggregation determined by ultrasonic scattering properties", Ultrasound Med. Biol., vol. 21, pp. 827-832, 1995.

[7] R. B. Ami, G. Barshtein, D. Zeltser, Y. Goldberg, I. Shapira, A. Roth, G. Keren, H. Miller, V. Prochorov, A. Eldor, S. Berliner and S. Yedgar, "Parameters of red blood cell aggregation as correlates of the inflammatory state", Am. J. Physiol. Heart Circ. Physiol., vol. 280, pp. H1982-H1988, 2001.

[8] D. Savery and G. Cloutier, "A point process approach to assess the frequency dependence of ultrasound backscattering by aggregating red blood cells", J. Acoust. Soc. Am., vol. 110, no. 6, pp. 3252-3262, 2001.

[9] I. Fontaine, D. Savery and G. Cloutier, "Simulation of ultrasound backscattering by red blood cell aggregates: effect of shear rate and anisotropy, Biophysical Journal, vol. 82, pp. 1696-1710, 2002.

[10] F. T. H. Yu and G. Cloutier, "Experimental ultrasound characterization of red blood cell aggregation using the structure factor size estimator", J. Acoust. Soc. Am., vol. 122, no. 1, pp. 645-656, 2007.

[11] R. K. Saha, E. Franceschini and G. Cloutier, "Assessment of accuracy of the structure-factor-size-estimator method in determining red blood cell aggregate size from ultrasound spectrum backscattering coefficient", J. Acoust. Soc. Am., vol. 129, no. 4, pp. 2269-2277, 2011.

[12] Franceschini E., Metzger B. and Cloutier G., "Forward problem study of an effective medium model for ultrasound blood characterization", IEEE Trans. ultras. Ferroelectr. Freq. Control., vol. 58, no. 12, pp. 2668-2679, 2011.

[13] "Handbook of hemorheology and hemodynamics", edited by O. K. Baskurt, M. R. Hardeman, M. W. Rampling and H. J. Meiselman (IOS Press, Amsterdam, Berlin, Oxford, Tokyo, Washington DC, 2007)

[14] H. Schmid-Schonbein, H. Malotta and F. Striesow, "Erythrocyte aggregation: causes, consequences and methods of assessment", Tijdschr NVKS, vol. 15, pp. 88-97, 1990.

[15] H. Schmid-Schonbein, G. Gallasch, J. V. Gosen, E. Volger and H. J. Klose, "Red cell aggregation in blood flow. I. New methods of quantification", Klin. Wschr., vol. 54, pp. 149-157, 1976.

[16] D. Savery and G. Cloutier, "High-frequency ultrasound backscattering by blood: Analytical and semi-analytical models of the erythrocyte cross section", J. Acoust. Soc. Am., vol. 23, no. 4, pp. 3963-3971, 2007.

[17] P. M. Morse and K. U. Ingard, "Theoretical Acoustics" (Princeton University Press, Princeton, NJ, 1968), Chap. 8, pp. 400-466.

[18] M. F. Insana and D. G. Brown, "Acoustic scattering theory applied to soft biological tissues", in *Ultrasonic Scattering in Biological Tissues*, edited by K. K. Shung and G. A. Thieme (CRC, Boca Raton, FL, 1993), Chap.4, pp. 76-124.

[19] I. Fontaine, M. Bertrand and G. Cloutier, "A system-based approach to modeling the ultrasound signal backscattered by red blood cells", Biophysical Journal, vol. 77, pp. 2387-2399, 1999.

[20] V. Twersky, "Low-frequency scattering by correlated distributions of randomly oriented particles", J. Acoust. Soc. Am., vol. 81, no. 5, pp. 1609-1618, 1987.

[21] K. K. Shung, “On the ultrasound scattering from blood as a function of hematocrit”, IEEE Trans. Sonics Ultrason. SU-29, pp. 327-331, 1982.

[22] A. Guinier and J. Fournet, “Small angle scattering of X-rays” (Wiley Interscience, New York 1955), Chap XIV, pp. 637-669.

[23] M. S. Wertheim, “Exact solution of the Percus-Yevick integral equation for hard spheres”, Physical Review Letters, vol. 10, no. 8, pp. 321-323, 1963.

[24] E. Franceschini and R. Guillermin, “Experimental assessment of four ultrasound scattering models for characterizing concentrated tissue-mimicking phantoms”, J. Acoust. Soc. Amer., vol. 132, pp. 3735-3747, 2012.

[25] C. C. Coussios, “The significance of shape and orientation in single-particle weak-scatterer models”, J. Acoust. Soc. Am., vol. 112, pp. 906-915, 2002.

[26] X. Weng, G. Cloutier, R. Beaulieu, G. O. Roederer, “Influence of acute-phase proteins on erythrocyte aggregation”, Am. J. Physiol., vol. 271, pp. H2346-H2352, 1996.

[27] E. Franceschini, F. T. H. Yu, F. Destrempes and G. Cloutier, “Ultrasound characterization of red blood cell aggregation with intervening attenuating tissue-mimicking phantoms”, J. Acoust. Soc. Am., vol. 127, pp. 1104-1115, 2010.

[28] F. T. H. Yu, J. K. Armstrong, J. Tripette, H. J. Meiselman and G. Cloutier, “A local increase in red blood cell aggregation can trigger deep vein thrombosis: Evidence based on quantitative cellular ultrasound imaging”, J. Thrombosis and Haemostasis, vol. 9, pp. 481-488, 2011.

[29] J. Tripette, A. Y. Denault, L. Allard, B. Chayer, L. P. Perrault and G. Cloutier, “Ultrasound monitoring of RBC aggregation as a real-time marker of the inflammatory response in a cardiopulmonary bypass swine model”, Critical Care Medicine, vol. 41, no. 8, pp. e171-e178, 2013.

[30] C. F. Tejero and J. A. Cuesta, “Hard-sphere and hard-disk freezing from the differential formulation of the generalized effective liquid approximation”, Physical Review E, vol. 47, no. 1, pp. 491-496, 1993.

[31] X. Guo and U. Riebel, “Theoretical direct correlation function for two-dimensional fluids of monodisperse hard spheres”, The Journal of Chemical Physics, vol. 125, 144504, 2006.

[32] N. W. Ashcroft, “Structure and resistivity of liquid metals”, Physical Review, vol. 145, pp. 83-90, 1966.

Emilie Franceschini received her M.S. degree in Mechanical Engineering from the Ecole Supérieure d'Ingénieurs de Marseille in 2003, and the Ph.D. degree in Acoustics from the University of Provence, Marseille, 2006. In 2007, she was a Postdoctoral Fellow at the Laboratory of Biorheology and Medical Ultrasonics, Research Center of the University of Montreal Hospital, Montreal, QC. Since October 2008, she is a Researcher at the French National Centre for Scientific Research (CNRS) in the Laboratory of Mechanics and Acoustics CNRS - UPR 7051, Marseille. Her current research interests include ultrasound imaging for biomedical applications, inverse problems and ultrasound characterization of biological tissues at the microscopic level. She is a member of the French Acoustical Society (SFA) and IEEE.

Ratan K. Saha obtained his B. Sc. in Physics (studied at A B N Seal College, Coochbehar, India) from the University of North Bengal, Siliguri, India in 1996 and received his M. Sc. in Physics from Jadavpur University, Kolkata, India in 1999. He carried out his Ph. D. work at the Saha Institute of Nuclear Physics, Kolkata during 2000-06. After that he joined the Laboratory of Biorheology and Medical Ultrasonics, Research Center of the University of Montreal Hospital, Montreal, Canada as a post-doctoral fellow (2007-08). He also worked as a post-doctoral fellow at Ryerson University, Toronto, Canada (2009-11). Since October 2011, he is a post-doctoral fellow at Saha Institute of Nuclear Physics and his current research interests include ultrasonic and photoacoustic characterizations of soft tissues.

Guy Cloutier (S'89-M'90-SM'07) obtained his B.Eng. in Electrical Engineering (84), and M.Sc. and Ph.D. in Biomedical Engineering (86, 90). Between the years 90-92, he was a post-doctoral fellow at The Pennsylvania State University with Prof. K. Kirk Shung. Prof. Cloutier is Director of the Laboratory of Biorheology and Medical Ultrasonics at the University of Montreal Hospital Research Center (www.lbum-crchum.com), and Professor of Radiology and Biomedical Engineering at the University of Montreal. His research interests are in quantitative ultrasound imaging of red blood cell aggregation, quasi-static and dynamic ultrasound elastography of atherosclerotic plaques, vascular aneurysms, deep vein thrombi and breast cancers, 3D morphologic and hemodynamic assessment of lower limb arterial stenoses, and mathematical and biomechanical modeling. He has published more than 130 peer-reviewed articles in these fields, holds 11 patents, and was recipient of the National Scientist award of the Fonds de Recherche en Santé du Québec (2004-2009).

TABLE CAPTION

Table I. Acoustical properties of blood found in [16] and [21].

Table II. Values of the aggregate radius and compactness used for computation of the simulated BSC_{SFM}, and values of parameters found with the SFSE. Aggregating conditions: r_{ag}/a varies, ϕ varies, ϕ_i=60% (except in the case of diaggregated RBCs where ϕ_i=100%). The parameter ϵ indicates the relative error.

TABLE I

	Density ρ (kg.m^{-3})	Compressibility κ (Pa^{-1})	Impedance Z (MRayl)
RBC	1092	3.41×10^{-10}	1.766
Plasma	1021	4.09×10^{-10}	1.580

TABLE II

SFM		ϕ=10%			ϕ=20%			ϕ=30%		
r_{ag}/a	ϕ_i (%)	W^*	R_g^*	$\epsilon_{R_g^*}$ (%)	W^*	R_g^*	$\epsilon_{R_g^*}$ (%)	W^*	R_g^*	$\epsilon_{R_g^*}$ (%)
1	100	0.61	0.39	-61.00	0.37	0.39	-61.00	0.17	0.38	-62.00
3.16	60	3.12	1.50	-52.53	3.29	1.56	-50.63	2.67	1.32	-58.23
5	60	7.41	3.81	-23.80	6.95	3.64	-27.20	5.31	3.04	-39.20
7.07	60	15.82	7.99	13.01	13.57	7.18	1.56	8.58	5.33	-24.61

FIGURE CAPTIONS

Figure 1. Frequency-dependent BSCs for different aggregate sizes and a constant aggregate compactness ϕ_i=60% at systemic hematocrits of 10, 20 and 30%. The symbols represent the BSC_{SFM} computation. The dashed lines represents the corresponding fitting with the SFSE, whereas the solid lines expresses the fitting with the EMTSFM.

Figure 2. a) Comparison of R_g^* estimated with SFSE and the actual aggregate size r_{ag}/a for the three systemic hematocrits 10, 20 and 30%. b) Linear relationships between W^* and R_g^*. Results presented here correspond to the configuration where r_{ag}/a varies and ϕ_i is fixed.

Figure 3. Frequency-dependent BSCs computed with the SFM for different aggregate compactnesses and a constant aggregate size r_{ag}/a=6.32 at systemic hematocrits of 10 and 20%, and corresponding fitting with the SFSE (in dashed lines) and with the EMTSFM (in solid lines).

Figure 4. a) Aggregate size R_g^* estimated with the SFSE as a function of different aggregate compactnesses for systemic hematocrits of 10 and 20%. The solid line represents the actual aggregate size r_{ag}/a=6.32. b) Linear relationships between W^* and R_g^*. Results presented here correspond to the configuration where ϕ_i varies and r_{ag}/a is fixed.

Figure 5. a) Values of r_{ag}^*/a and ϕ_i^* estimated by the EMTSFM as a function of the actual aggregate radius for the three systemic hematocrits of 10, 20 and 30%. Also represented are actual values of r_{ag}/a and ϕ_i. (b) Corresponding relative errors of r_{ag}^*/a and ϕ_i^*.

Figure 6. a) Values of r_{ag}^*/a and ϕ_i^* estimated by the EMTSFM as a function of the actual aggregate compactness for the systemic hematocrits of 10 and 20%. Also represented are actual values of r_{ag}/a and ϕ_i. (b) Corresponding relative errors of r_{ag}^*/a and ϕ_i^*.

Figure 7. Frequency-dependent BSCs computed with the SFM for different aggregate sizes and a constant aggregate compactness ϕ_i=60% at systemic hematocrits of 10, 20 and 30%, and corresponding fitting with the GM.

Figure 8. a) Values of a_{eff}^*/a and ϕ_i^* estimated by the GM as a function of the actual aggregate radius for the three systemic hematocrits of 10, 20 and 30%. Also represented are actual values of r_{ag}/a and ϕ_i. (b) Corresponding relative errors of a_{eff}^*/a and ϕ_i^*.

Figure 9. a) Values of a_{eff}^*/a and ϕ_i^* estimated by the GM as a function of the actual aggregate compactness for the systemic hematocrits of 10 and 20%. Also represented are actual values of r_{ag}/a and ϕ_i. (b) Corresponding relative errors of a_{eff}^*/a and ϕ_i^*.

Figure 10. Logarithm of the error between the simulated BSC_{SFM} and the fitted curves with the three scattering models GM, SFSE and EMTSFM. a) As a function of the actual aggregate size for the clustering configuration where r_{ag}/a varies and ϕ_i is fixed. b) As a function of the actual aggregate compactness for the clustering configuration where ϕ_i varies and r_{ag}/a is fixed.

Figure 11. a) Concentration of aggregated RBCs ϕ' as a function of the mean aggregate radius r_{ag}/a for the three systemic hematocrits of 20, 30 and 40%. b) and c) Frequency-dependent BSCs computed with the SFM in the 3D case for different aggregate sizes and a constant aggregate compactness ϕ_i=74% at systemic hematocrits of 30 and 40%, and corresponding fitting with the SFSE model, the EMTSFM and the GM.

Figure 12. a) Values of r^*_{ag}/a and ϕ^*_i estimated by the EMTSFM as a function of the actual aggregate radius for the three systemic hematocrits of 20, 30 and 40%. Also represented are actual values of r_{ag}/a and ϕ_i. (b) Corresponding relative errors of r^*_{ag}/a and ϕ^*_i.

Figure 13. a) Values of a^*_{eff}/a and ϕ^*_i estimated by the GM as a function of the actual aggregate radius for the three systemic hematocrits of 20, 30 and 40%. Also represented are actual values of r_{ag}/a and ϕ_i. (b) Corresponding relative errors of a^*_{eff}/a and ϕ^*_i.

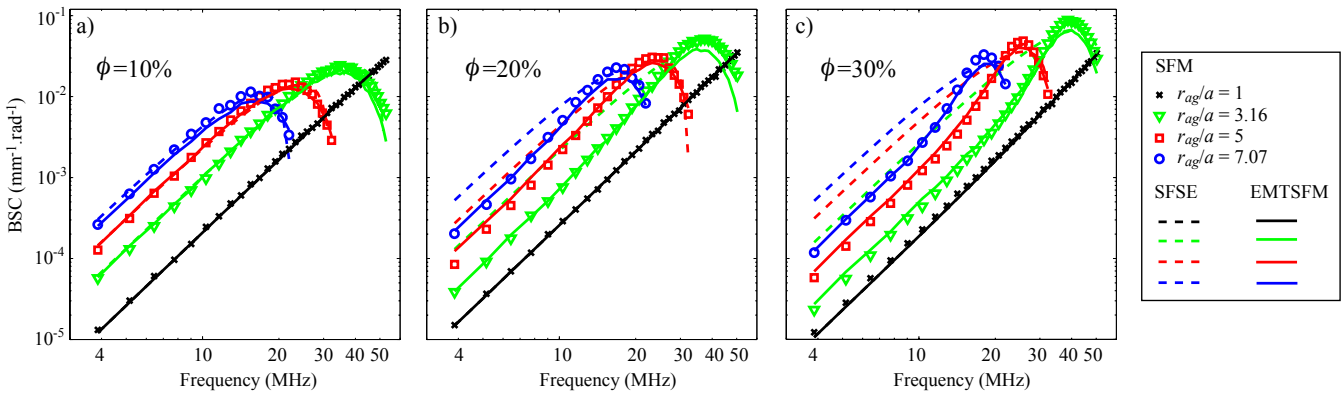
a)
ϕ=10%
b)
ϕ=20%
c)
ϕ=30%
BSC (mm^{-1}.rad^{-1})
10^{-1}
10^{-2}
10^{-3}
10^{-4}
10^{-5}
4
10
20
30
40
50
Frequency (MHz)
SFM
r_{ag}/a = 1
r_{ag}/a = 3.16
r_{ag}/a = 5
r_{ag}/a = 7.07
SFSE
EMTSFM

Fig. 1.

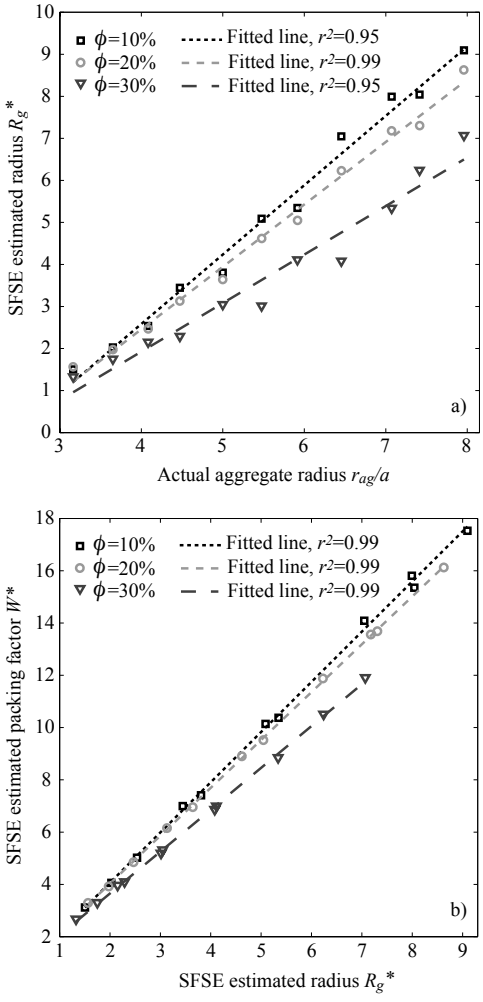
ϕ=10%
Fitted line, r²=0.95
ϕ=20%
Fitted line, r²=0.99
ϕ=30%
Fitted line, r²=0.95
SFSE estimated radius Rg*
Actual aggregate radius rag/a
a)
ϕ=10%
Fitted line, r²=0.99
ϕ=20%
Fitted line, r²=0.99
ϕ=30%
Fitted line, r²=0.99
SFSE estimated packing factor W*
SFSE estimated radius Rg*
b)

Fig. 2.

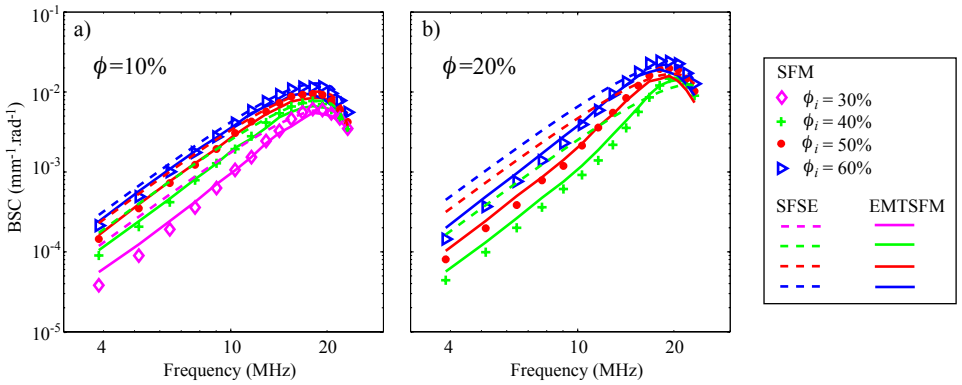
a)
ϕ=10%
b)
ϕ=20%
BSC (mm^{-1} rad^{-1})
10^{-1}
10^{-2}
10^{-3}
10^{-4}
10^{-5}
4
10
20
Frequency (MHz)
Frequency (MHz)
SFM
ϕ_i = 30%
ϕ_i = 40%
ϕ_i = 50%
ϕ_i = 60%
SFSE
EMTSFM

Fig. 3.

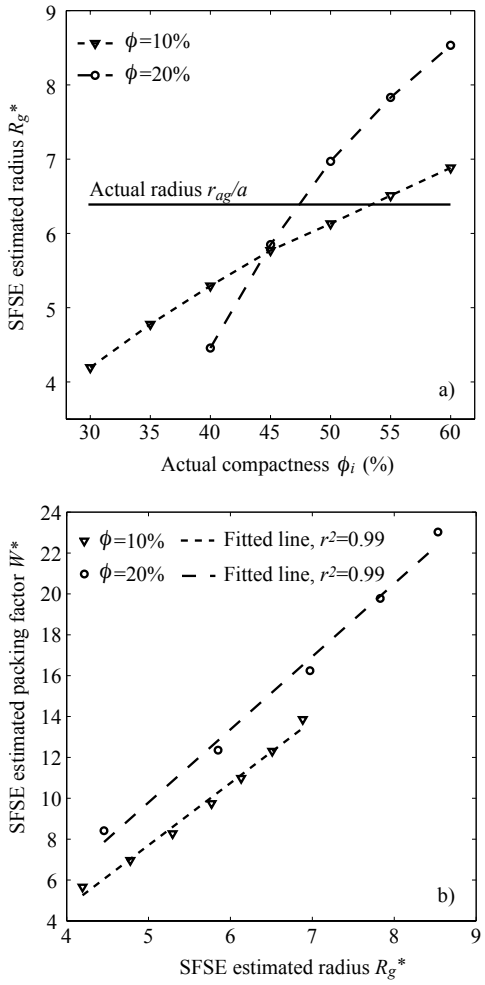
ϕ=10%
ϕ=20%
Actual radius r_{ag}/a
SFSE estimated radius R_g^*
Actual compactness ϕ_i (%)
a)
ϕ=10% Fitted line, r^2=0.99
ϕ=20% Fitted line, r^2=0.99
SFSE estimated packing factor W^*
SFSE estimated radius R_g^*
b)

Fig. 4.

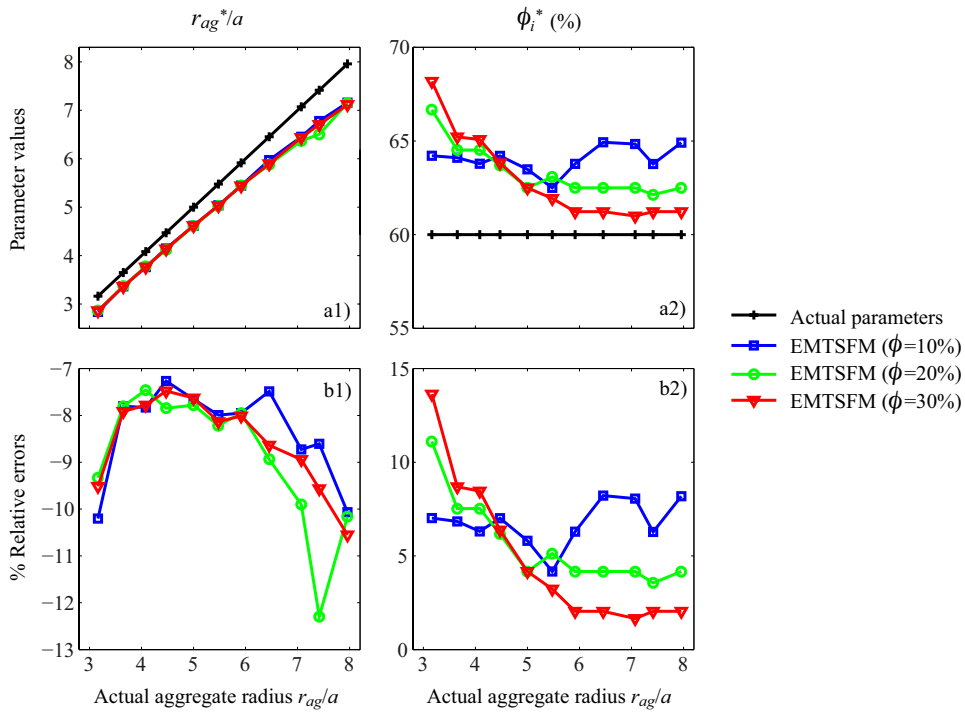
r_{ag}^*/a
ϕ_i^* (%)
Parameter values
% Relative errors
a1)
a2)
b1)
b2)
Actual aggregate radius r_{ag}/a
Actual aggregate radius r_{ag}/a
Actual parameters
EMTSFM (ϕ=10%)
EMTSFM (ϕ=20%)
EMTSFM (ϕ=30%)

Fig. 5.

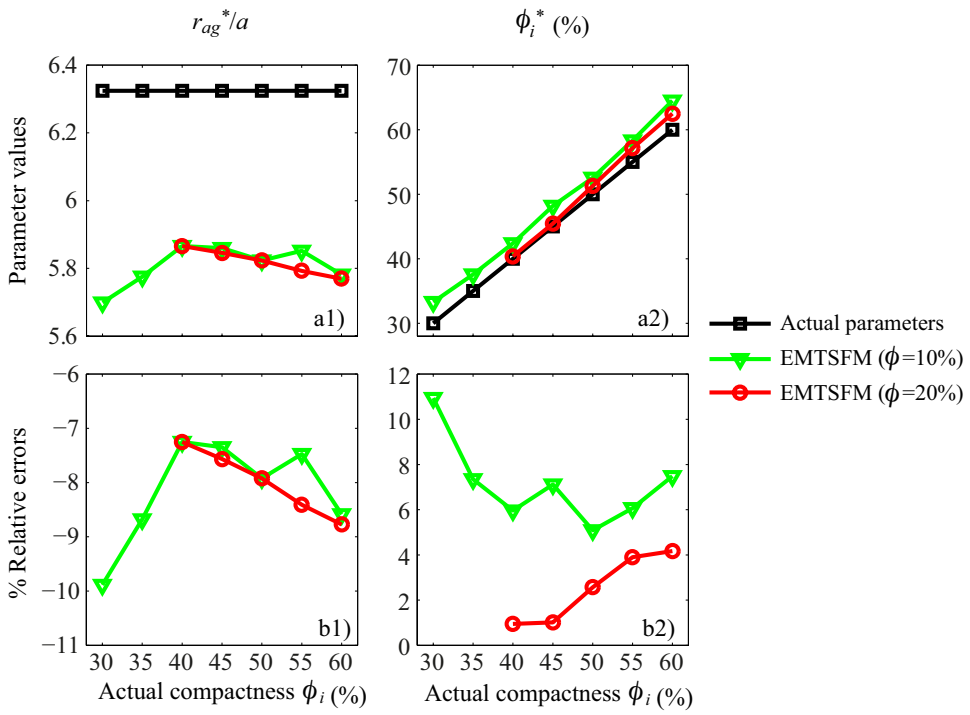
r_{ag}^*/a
ϕ_i^* (%)
Parameter values
% Relative errors
a1)
a2)
b1)
b2)
Actual compactness ϕ_i (%)
Actual compactness ϕ_i (%)
Actual parameters
EMTSFM (ϕ=10%)
EMTSFM (ϕ=20%)

Fig. 6.

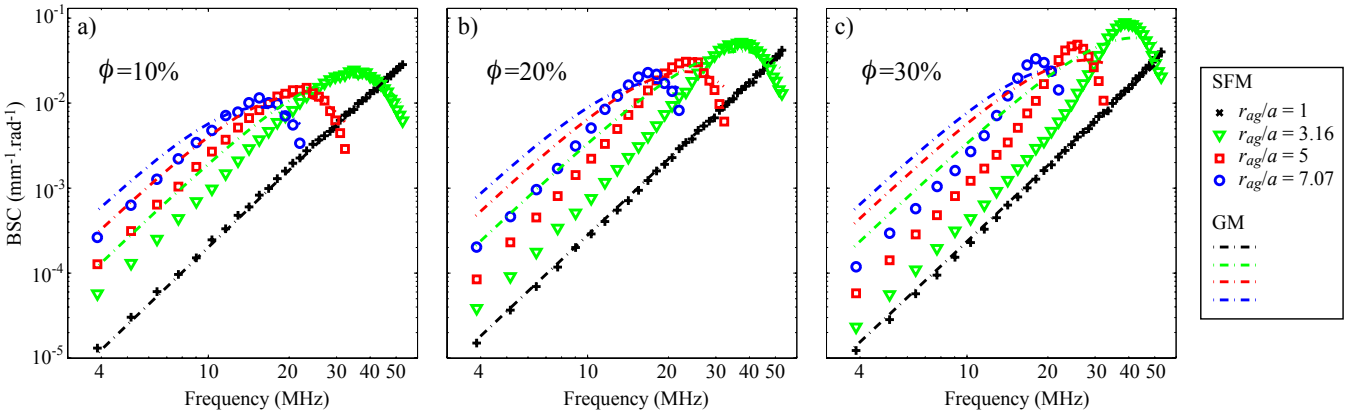
a)
ϕ=10%
b)
ϕ=20%
c)
ϕ=30%
BSC (mm^{-1}.rad^{-1})
10^{-1}
10^{-2}
10^{-3}
10^{-4}
10^{-5}
4
10
20
30
40
50
Frequency (MHz)
SFM
r_{ag}/a = 1
r_{ag}/a = 3.16
r_{ag}/a = 5
r_{ag}/a = 7.07
GM

Fig. 7.

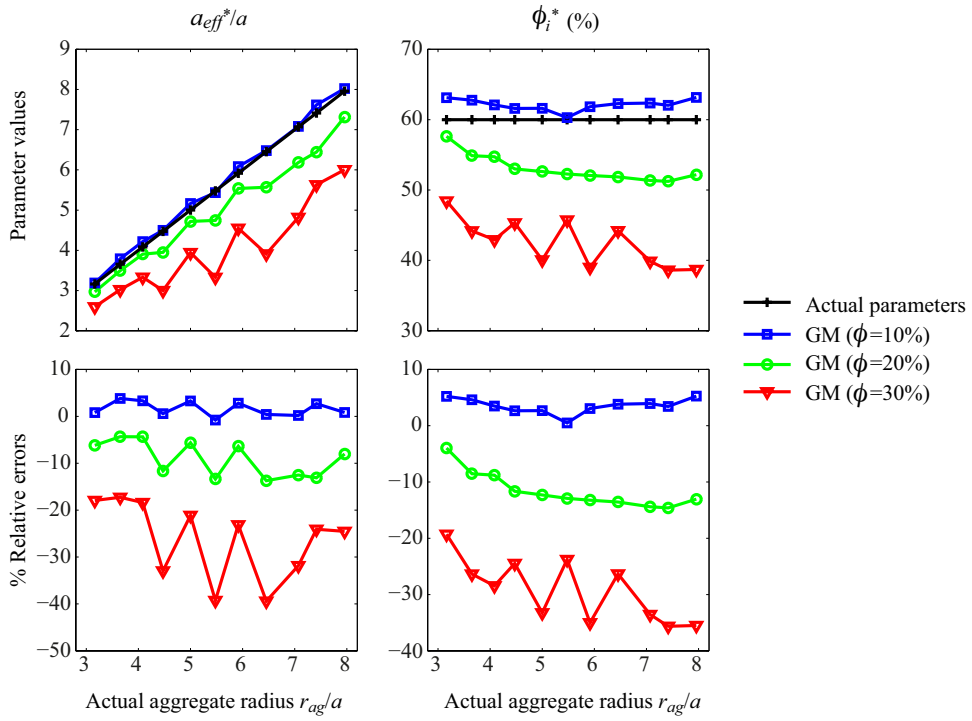
a_{eff}^*/a
ϕ_i^* (%)
Parameter values
% Relative errors
Actual aggregate radius r_{ag}/a
Actual aggregate radius r_{ag}/a
Actual parameters
GM (ϕ=10%)
GM (ϕ=20%)
GM (ϕ=30%)

Fig. 8.

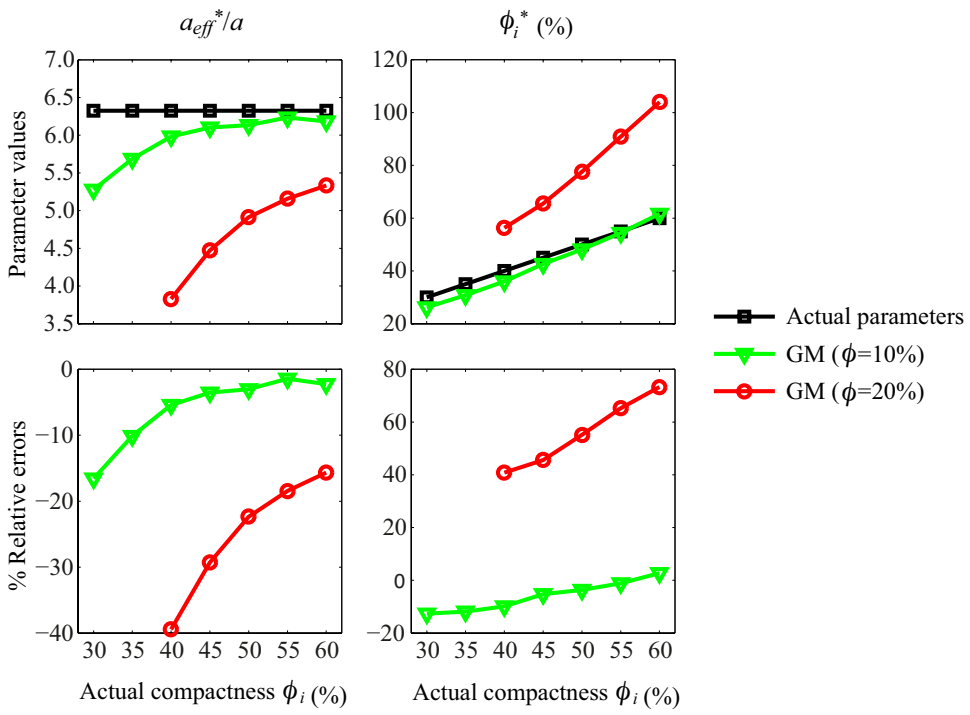
a_{eff}^*/a
ϕ_i^* (%)
Parameter values
% Relative errors
Actual compactness ϕ_i (%)
Actual compactness ϕ_i (%)
Actual parameters
GM (ϕ=10%)
GM (ϕ=20%)

Fig. 9.

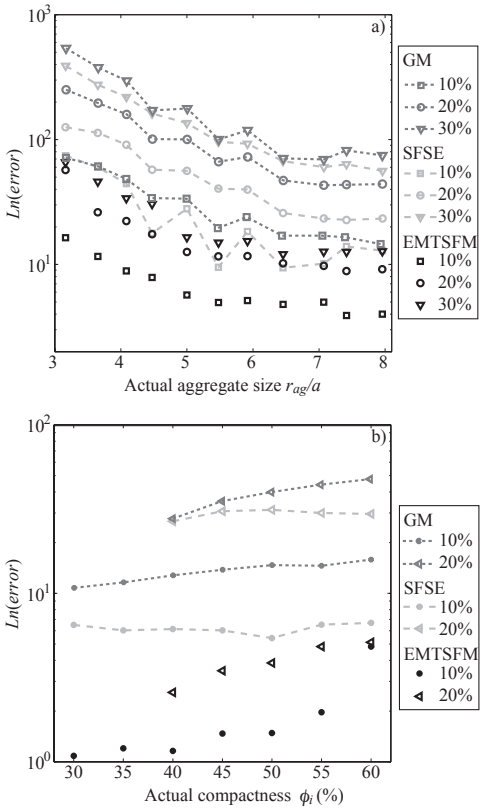
a)
Ln(error)
Actual aggregate size r_{ag}/a
GM
10%
20%
30%
SFSE
10%
20%
30%
EMTSFM
10%
20%
30%
b)
Ln(error)
Actual compactness ϕ_i (%)
GM
10%
20%
SFSE
10%
20%
EMTSFM
10%
20%

Fig. 10.

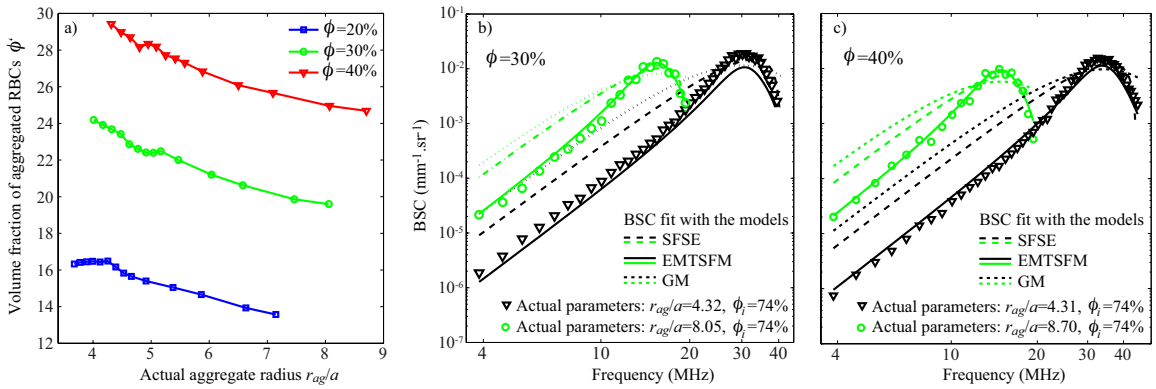
a)
ϕ=20%
ϕ=30%
ϕ=40%
Volume fraction of aggregated RBCs ϕ'
Actual aggregate radius r_{ag}/a
b)
ϕ=30%
BSC (mm^{-1}.sr^{-1})
BSC fit with the models
SFSE
EMTSFM
GM
Actual parameters: r_{ag}/a=4.32, ϕ_i=74%
Actual parameters: r_{ag}/a=8.05, ϕ_i=74%
Frequency (MHz)
c)
ϕ=40%
BSC fit with the models
SFSE
EMTSFM
GM
Actual parameters: r_{ag}/a=4.31, ϕ_i=74%
Actual parameters: r_{ag}/a=8.70, ϕ_i=74%
Frequency (MHz)

Fig. 11.

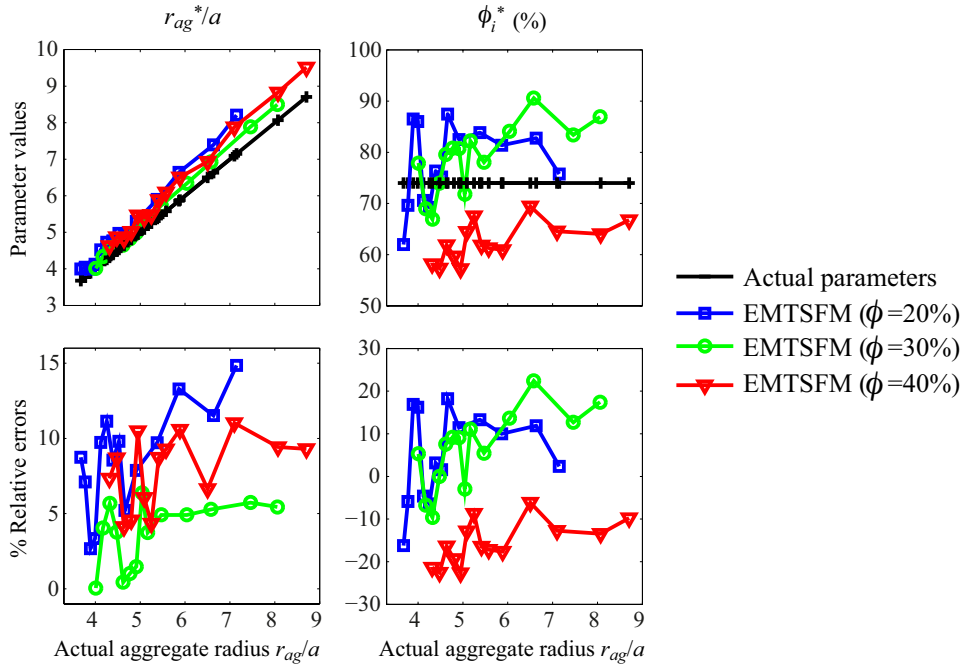
r_{ag}^*/a
ϕ_i^* (%)
Parameter values
% Relative errors
Actual aggregate radius r_{ag}/a
Actual aggregate radius r_{ag}/a
Actual parameters
EMTSFM (ϕ=20%)
EMTSFM (ϕ=30%)
EMTSFM (ϕ=40%)

Fig. 12.

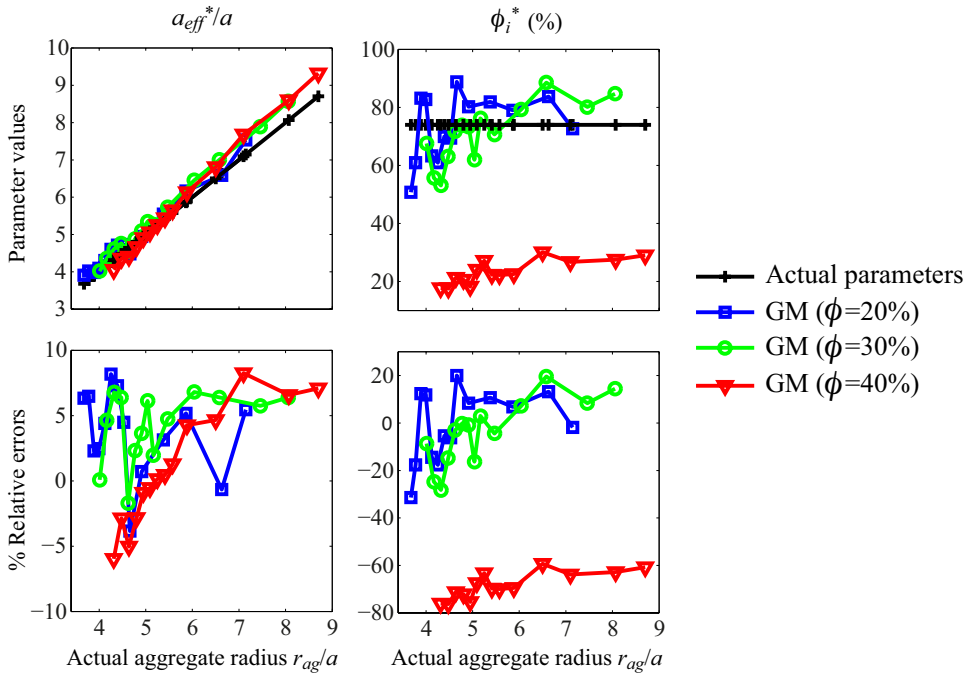
a_{eff}^*/a
ϕ_i^* (%)
Parameter values
% Relative errors
Actual aggregate radius r_{ag}/a
Actual aggregate radius r_{ag}/a
Actual parameters
GM (ϕ=20%)
GM (ϕ=30%)
GM (ϕ=40%)

Fig. 13.